Dynamic and Thermodynamic Characteristics of Atmospheric Response to Anomalous Sea-Ice Extent in the Sea of Okhotsk

MEIJI HONDA

Institute for Global Change Research, Frontier Research System for Global Change, Tokyo, Japan

KOJI YAMAZAKI

Graduate School of Environmental Earth Science, Hokkaido University, Sapporo, Japan

HISASHI NAKAMURA

Institute for Global Change Research, Frontier Research System for Global Change, and Department of Earth and Planetary Physics, University of Tokyo, Tokyo, Japan

KENSUKE TAKEUCHI

Institute of Low Temperature Science, Hokkaido University, Sapporo, Japan

(Manuscript received 24 September 1998, in final form 1 February 1999)

ABSTRACT

Influence of sea-ice extent anomalies within the Sea of Okhotsk on the large-scale atmospheric circulation is investigated through an analysis of the dynamic and thermodynamic characteristics of the response in an atmospheric general circulation model to specified anomalous sea-ice cover. Significant response appears not only around the Sea of Okhotsk, but also downstream over the Bering Sea, Alaska, and North America in the form of a stationary wave train in the troposphere. This remote response, associated with wave activity flux emanating from the Okhotsk area to the downstream, is regarded as a stationary Rossby wave generated thermally by the anomalous turbulent heat fluxes from the ocean surface as a result of the anomalous sea-ice cover. The Pacific storm track in the model that extends zonally at 35°N is located too far south of the Sea of Okhotsk to exert substantial feedback forcing on the local and remote response. Since a similar stationary wave train is identified in the composite difference fields of the observed data between heavy and light ice years, it is believed that the model appropriately reproduces the real atmospheric response to the Okhotsk sea-ice extent anomalies. Simulated seesaws in the meridional surface wind and surface air temperature anomalies between the eastern Sea of Okhotsk and eastern Bering Sea associated with the local and remote response, respectively, to the Okhotsk sea-ice anomalies seem to be consistent with the observed seesaw in the anomalous sea-ice cover between these maritime regions. There is a hint of reinforcement of the remote response around the Alaskan Pacific coast through destabilization of barotropic Rossby waves due to the thermal damping effect associated with the anomalous atmosphere–ocean heat exchange both in the model and real atmosphere.

1. Introduction

The Sea of Okhotsk, which extends as far south as 45°N, is the southernmost ocean in the Northern Hemisphere that is covered with sea ice during winter. The interannual variability in the atmospheric circulation is known to cause large fluctuations in the sea-ice cover within the Sea of Okhotsk. Aso (1986) suggested that the interannual variability in the Okhotsk sea-ice cover might be influenced by changes in the cyclone paths associated with large-scale stationary anomalies in the atmospheric circulation. Fluctuations in the Okhotsk sea-ice cover were also shown to be associated with anomalous positions and/or intensities of the Siberian high and the Aleutian low (Cavalieri and Parkinson 1987; Parkinson 1990). Fang and Wallace (1994) showed that changes in the Okhotsk sea-ice cover tend to lag the atmospheric anomalies by a week, suggestive of the atmospheric control of the sea-ice cover. The presence of significant influence of large-scale atmospheric circulation on sea-ice cover has also been suggested in several other maritime regions (Crane 1978;

Corresponding author address: Dr. Meiji Honda, Institute for Global Change Research, Frontier Research System for Global Change, SEAVANS North 7F, 1-2-1 Shibaura, Minato-Ku, Tokyo 105-6791, Japan.
E-mail: meiji@frontier.esto.or.jp

Rogers 1978; Walsh and Johnson 1979; Niebauer 1980; Walsh and Sater 1981; Overland and Pease 1982; Agnew 1993).

Little has been known, however, about whether or not anomalous sea-ice cover, in turn, exerts any influence upon the atmospheric circulation. The presence of sea ice substantially reduces heat and moisture fluxes from the sea surface and it consequently acts to cool the air above. It is conjectured that observed changes in the sea-ice cover within the Sea of Okhotsk could substantially alter the distribution of the fluxes, which may cause feedback to the atmosphere. Although the local influence of the Okhotsk sea-ice extent on the atmosphere around Hokkaido Island of Japan has been examined extensively (e.g., Nagata and Ikawa 1988; Sasaki and Deguti 1988; Honda et al. 1994; Okubo and Mannoji 1994), its large-scale influence has received limited study. Using an atmospheric general circulation model (AGCM), Herman and Johnson (1978) studied the sensitivity of the atmospheric circulation to the variability in the Northern Hemisphere circumpolar sea-ice boundary, including the Sea of Okhotsk. Although their model results indicate that the atmospheric response to the hypothetical maximum boundary differs substantially from that to the minimum boundary setting, the difference in the response was exaggerated because of their unrealistic setting of the sea-ice boundary.

The purpose of this paper is to examine the response of the large-scale atmospheric circulation solely to the Okhotsk sea-ice cover anomalies, and to understand its dynamic and thermodynamic characteristics. We first analyze the atmospheric response simulated in an AGCM in order to identify the sea-ice influence on the atmosphere. Differences in the simulated atmospheric anomalies between the heavy and light ice cases can be interpreted as being forced by the sea-ice extent anomalies, because they are specified in this set of model experiments, which allows no atmospheric feedback to the model sea-ice cover. Then, an attempt is made to extract the atmospheric anomalies associated with the anomalous sea-ice cover in the Sea of Okhotsk from the observational data. Some preliminary results of our AGCM experiment have been reported in Honda et al. (1996).

2. AGCM experiment

a. Model and experimental design

The AGCM used in the present study is a global primitive equation model with a spectral transform method, developed at the Meteorological Research Institute of the Japan Meteorological Agency and implemented at Hokkaido University (e.g., Chiba et al. 1996). We use a particular version of the model with 30 vertical levels and triangular truncation at wavenumber 21, which corresponds approximately to 5.625° resolution both in latitude and longitude (T21L30). The distributions of sea surface temperature (SST) and sea-ice cover in the model were prescribed as their climatological means based on the observed monthly mean data. The sea-ice concentration is assumed to be either 100% or 0% and ice thickness to be 1 m at any location where ice exists. Surface temperature and snow depth over sea ice or land surface, and surface heat and momentum fluxes are predicted in the model. The fluxes were calculated based on Louis's (1979) parameterization.

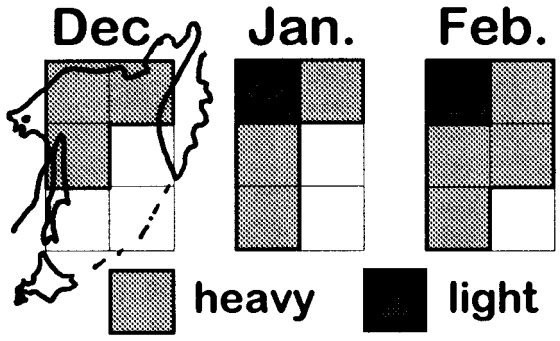

FIG. 1. Sea ice settings as the model boundary condition of the heavy and light ice cases for the Sea of Okhotsk from Dec to Feb (left to right). In the heavy ice case, all grid boxes with shading are assumed to be covered with ice, whereas only the grid box in the northwestern Okhotsk (with dense shading) is ice covered in Jan and Feb and completely ice free in Dec in the light ice case. Geographical alignment of the five model grid boxes within the Sea of Okhotsk is shown in the left panel (after Honda et al. 1996).

Sensitivity experiments of the atmospheric response to the Okhotsk sea-ice cover anomalies were carried out as follows. First, a control run was performed for eight years under the climatological mean sea-ice condition. Then, we prepared two sets of the model boundary condition in the Sea of Okhotsk based on the observed extreme conditions of heavy and light sea-ice cover (Fig. 1). In order to extract a clear signal of the atmospheric response to the Okhotsk sea-ice anomalies, we exaggerated the ratio of the heavy versus light ice extent in the model, which is about twice as large as what was observed. Otherwise, the same boundary conditions were set as in the control run. We adopted the atmospheric condition at the end of November in the fifth model year to the initial condition for the pair of integrations for the heavy and light ice cases. The integration with each of these settings was repeated five times with slightly different atmospheric initial conditions. Then, the ensemble mean of the five integrations was analyzed as follows, in order to suppress noise due to the initial condition dependency and to assess the robustness of the results. We focus mainly upon the differences in atmospheric field (heavy minus light) of the ensemble January–February means, which was found to be significant and, hence, was regarded as a meaningful model response.

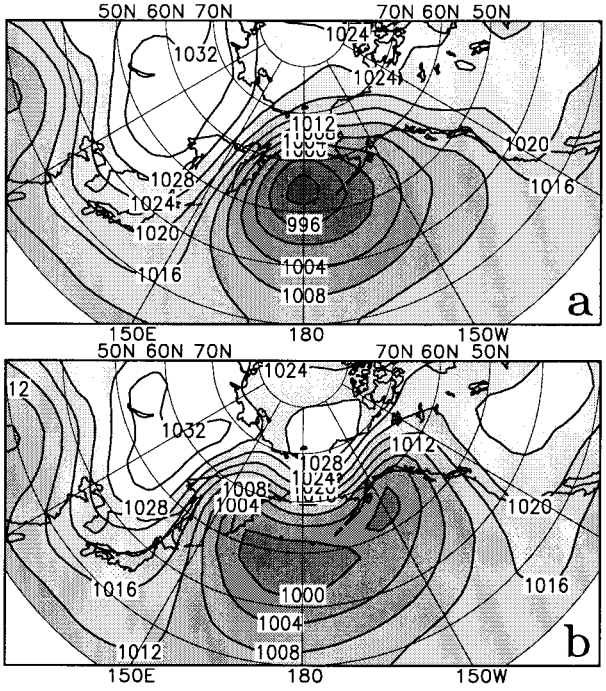

FIG. 2. AGCM-simulated Jan–Feb mean sea level pressure (hPa) fields over the North Pacific, obtained as averages of the five integrations both for the (a) heavy and (b) light ice cases.

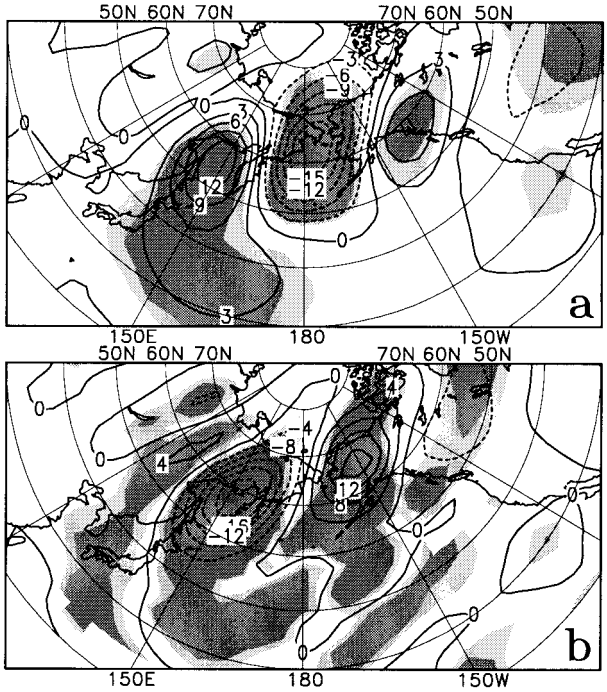

FIG. 4. AGCM response for Jan–Feb mean in (a) sea level pressure (hPa) and (b) surface air temperature (°C) to the Okhotsk sea-ice anomalies. Each of the difference maps has been obtained by subtracting the composite response for the five light-case simulations from that for the five heavy-case ones. Areas of light and heavy shading indicate the differences with 95% and 99% confidence levels, respectively, based on the *t* statistic (after Honda et al. 1996).

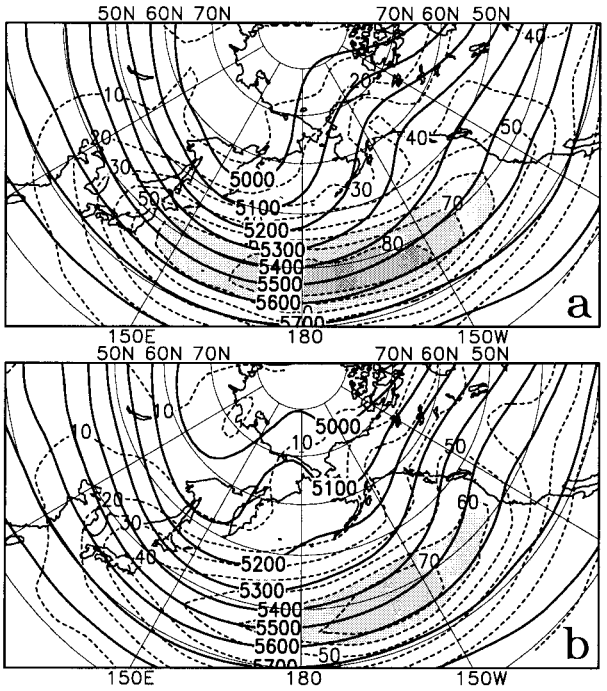

FIG. 3. As in Fig. 2, but for 500-hPa geopotential height (m; thick lines), superimposed on the variance of the 500-hPa meridional velocity ($\overline{v'^2}$) associated with transient eddies with periods shorter than 6 days ($m^2\ s^{-2}$; thin dashed lines with shading for more than 50 $m^2\ s^{-2}$).

b. Results of numerical experiment

In the model-simulated mean sea level pressure (SLP) fields for January–February for the heavy and light ice cases, the most notable difference appears in the intensity of the Aleutian low and Beaufort high to the north (Fig. 2). The Aleutian low is substantially deeper in the heavy ice case, and the center is located around where it is in the control run. In the light ice case, in contrast, the low is weakened and split into two cells. In the corresponding 500-hPa geopotential height (Z_{500}) field for the heavy ice case, a trough over the Kamchatka peninsula is deepened markedly (Fig. 3a), whereas in the light ice case the trough is weakened and almost split into two branches, one over the Sea of Okhotsk and the other over the Bering Strait (Fig. 3b).

To isolate the atmospheric responses to the sea-ice anomalies, we calculated the difference field by subtracting the model response for the light ice simulation from that for the heavy ice one. Since the composite response to each of the heavy and light ice extents was found to be more or less ''linear'' (i.e., with similar patterns and magnitudes but sign reversed), the difference corresponds roughly to twice the model response for the heavy ice case. At the surface, the Sea of Okhotsk is covered with anticyclonic anomalies (Fig. 4a) and anomalous cold air (Fig. 4b). These anomalies over the

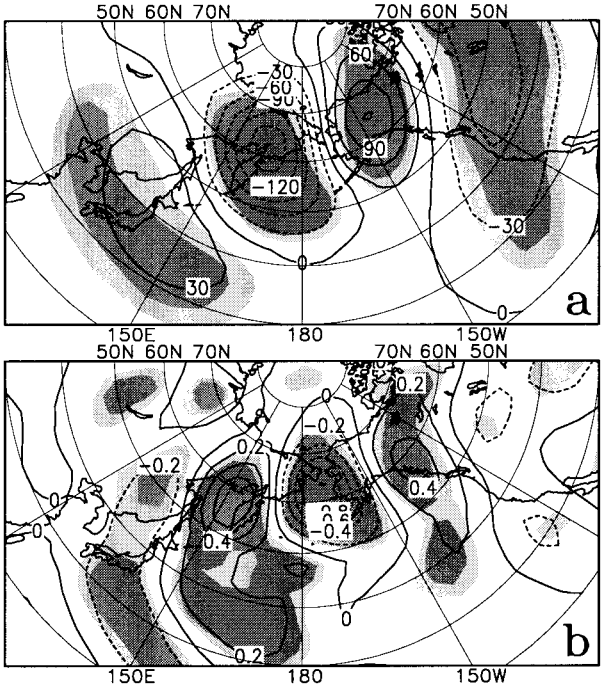

FIG. 5. As in Fig. 4, but for 500-hPa (a) geopotential height (m) and (b) p velocity (ω: 10^{-1} Pa s^{-1}).

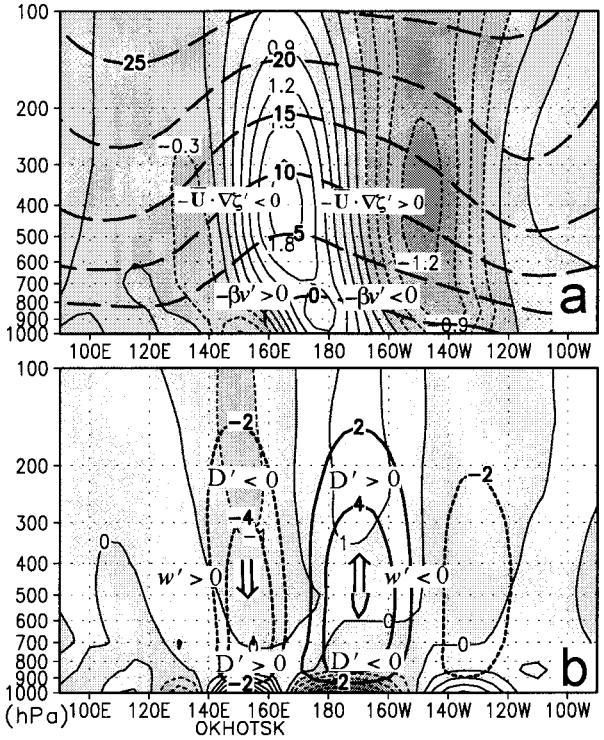

FIG. 6. (a) Zonal cross sections averaged over 50°–70°N of AGCM-simulated Jan–Feb mean differences between the heavy and light ice cases of the relative vorticity (10^{-5} s^{-1}; thin lines with dark shading for negative values), superimposed on the basic-state westerly wind speed (m s^{-1}; thick long dashed lines). (b) As in (a) but for the divergence difference (10^{-6} s^{-1}; thin lines with dark shading for negative values), superimposed on the vertical-motion wind difference (10^{-3} m s^{-1}; thick lines). The Sea of Okhotsk roughly corresponds to 140°–160°E.

Sea of Okhotsk are statistically significant based on the Student's t-test. Furthermore, significant wavelike anomalies extend downstream toward North America roughly along a great circle that passes the Sea of Okhotsk. Similar wavelike anomalies are evident also in the mid- and upper troposphere (Fig. 5). The Z_{500}-anomaly pattern shifts westward by about a quarter wavelength relative to the SLP anomaly pattern, which reflects the baroclinic nature of the response particularly in the lower troposphere (Fig. 6a). In Figs. 5b and 6, anomalous midtropospheric descent (ascent) to the west (east) of the cyclonic anomalies is in conjunction with anomalous upper-tropospheric convergence (divergence) and near-surface divergence (convergence). The downstream anomalies, which are much stronger than the upstream ones, may be regarded as a stationary Rossby wave train generated around the Sea of Okhotsk, whose group velocity is eastward.

We investigate dynamic and thermodynamic properties of this wavy stationary response, assessing the primary balance in the vorticity and thermodynamic equations. The three-dimensional structure of a stationary Rossby wave embedded in the basic baroclinic westerlies is maintained in balance between the horizontal vorticity advection and divergence/convergence effect associated with the vertical motion. For a large-scale motion, the vorticity equation may be written as

$$\frac{\partial \zeta}{\partial t} = -\mathbf{U} \cdot \boldsymbol{\nabla}(f + \zeta) - (f + \zeta)D + F, \qquad (1)$$

with

$$D = \boldsymbol{\nabla} \cdot \mathbf{U},$$

where ζ is the relative vorticity, f the Coriolis parameter, $\mathbf{U}$ the horizontal wind velocity, and F the forcing term. The atmospheric responses in the heavy and light ice cases can approximately be regarded as small-amplitude perturbations from the basic state defined as the mean over the last four years of the control run. Then, (1) may be linearlized for small-amplitude steady perturbation as

$$0 \equiv \frac{\partial \zeta'}{\partial t}$$
$$= -\overline{\mathbf{U}} \cdot \boldsymbol{\nabla}\zeta' - \mathbf{U}' \cdot \boldsymbol{\nabla}(f + \overline{\zeta}) - (f + \overline{\zeta})D' + F', \quad (2)$$

where primes denote perturbation quantities (i.e., anomalies) and overbars indicate the basic state. In (2), F' includes the effect of friction, dissipation, and anomalous feedback from transient eddies. We computed each of the terms in (2) based on the composite difference anomalies. The three top panels of Fig. 7 show the distribution of the first three terms in (2) in the cross section along the path of the wave train. The sum of these terms, which corresponds to $-F'$ (Fig. 7d), is generally much

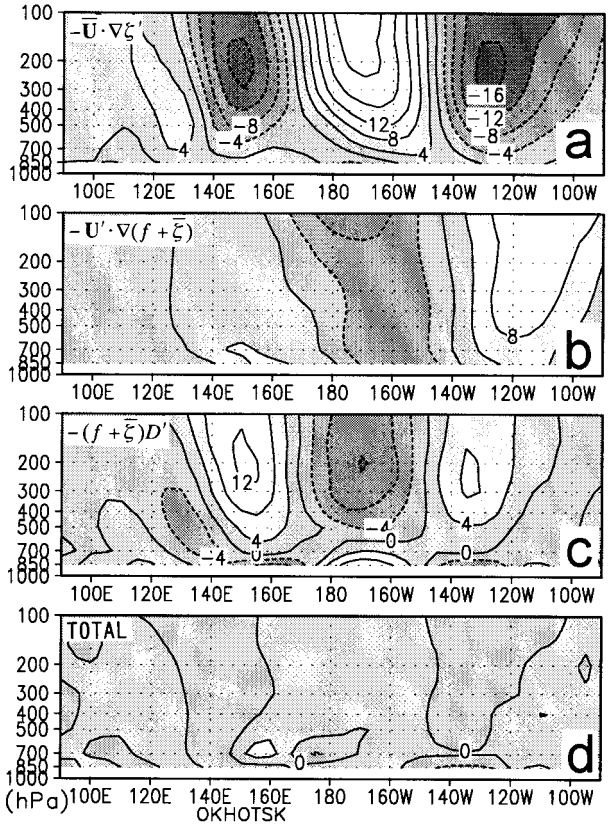

FIG. 7. As in Fig. 6, but for (a) the advection of vorticity anomalies by the basic flow, (b) advection of the basic-state absolute vorticity by meridional wind anomalies (mainly $-\beta_e v'$), (c) vortex-tube stretching associated with the anomalous divergence, and (d) the sum of (a), (b), and (c). Units: 10^{-6} s^{-1} day^{-1}.

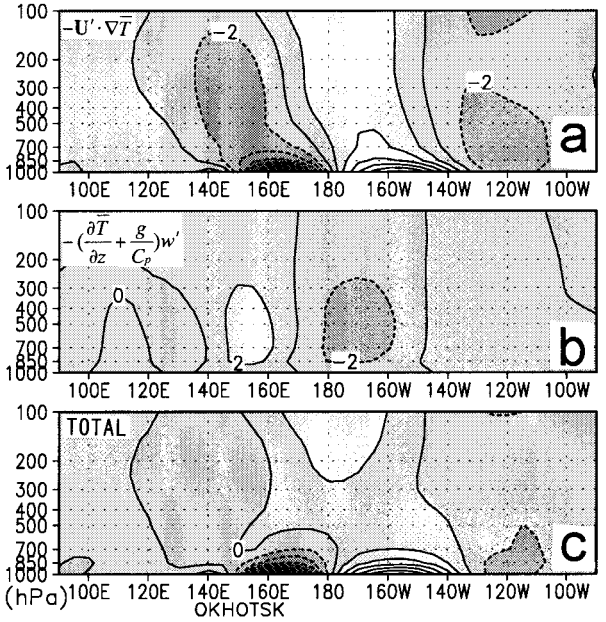

FIG. 8. As in Fig. 6, but for (a) the advection of the basic-state temperature by horizontal wind anomalies, (b) adiabatic heating associated with anomalous vertical motion, and (c) the sum of (a) and (b). Units: °C day^{-1}.

smaller than each of the other three terms, indicating that the friction and transient effects are of secondary importance. This indicates that the stationary model response is subject to low-frequency dynamics, with no significant atmospheric feedback from the transients. In fact, the Pacific storm track extends zonally around 35°N (Fig. 3), located too far south to exert significant feedback forcing on the wave train propagating along ~60°N. It is apparent that the primary balance in the vorticity budget is quite different between near the surface and aloft. In the mid- and upper troposphere, the prevailing westerlies in the basic state render the zonal ζ' advection dominant over the planetary vorticity advection, and the former is balanced primarily with the divergence effect (Figs. 6, 7a,c), that is,

$$-\overline{\mathbf{U}}\cdot\nabla\zeta' - (f+\overline{\zeta})D' \approx 0. \tag{3}$$

As the ζ' advection diminishes due to the weak westerlies near the surface (Fig. 7a), the divergence effect is balanced primarily with the advection of the basic-state absolute (mainly planetary) vorticity (Figs. 6, 7b,c), that is,

$$-\beta_e v' - (f+\overline{\zeta})D' \approx -\mathbf{U}'\cdot\nabla(f+\overline{\zeta}) - (f+\overline{\zeta})D' \approx 0 \tag{4}$$

with

$$\beta_e = \frac{\partial(f+\overline{\zeta})}{\partial y},$$

where v' is the anomalous meridional wind component.

The thermodynamic equation may be written as

$$\frac{\partial T}{\partial t} = -\mathbf{U}\cdot\nabla T - \left(\frac{\partial T}{\partial z}+\frac{g}{C_p}\right)w + \frac{J}{C_p}, \tag{5}$$

where T is the air temperature, w the vertical velocity, C_p the specific heat at constant pressure, g the acceleration of gravity, and J the heating rate due to diabatic effects and heat flux convergence associated with transient eddies. For small-amplitude steady anomalies, (5) may be linearlized as

$$0 \equiv \frac{\partial T'}{\partial t} = -\mathbf{U}'\cdot\nabla\overline{T} - \left(\frac{\partial\overline{T}}{\partial z}+\frac{g}{C_p}\right)w' + \frac{J'}{C_p}. \tag{6}$$

Here, the equation has been somewhat simplified based on the fact that the advection of temperature anomalies by the basic flow ($-\overline{\mathbf{U}}\cdot\nabla T'$) was found to be of secondary importance in the simulated response. So was the anomalous heat flux convergence associated with transient eddies in J'. We plotted the first two terms on the right-hand side in the zonal–vertical cross section (Figs. 8a and 8b). Except near the surface, the primary balance is achieved between the horizontal temperature

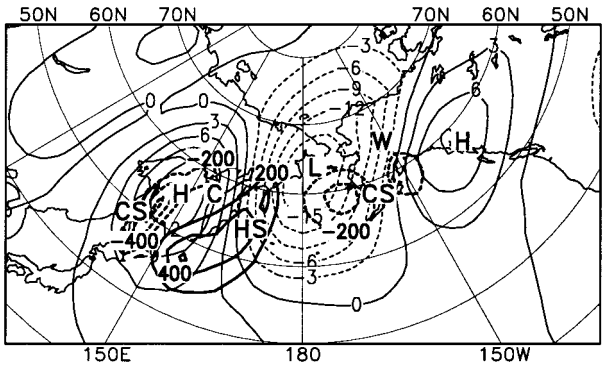

FIG. 9. As in Fig. 4, but for anomalous surface fluxes of sensible and latent heat combined (W m^{-2}; positive: upward), superimposed on the sea level pressure anomaly (hPa; thinner lines). H: anomalous high, L: anomalous low, C: anomalous cold air, W: anomalous warm air, CS: cooling source, and HS: heating source.

advection by the perturbation flow and adiabatic heating/cooling associated with the perturbation descent/ascent (Fig. 8c), that is,

$$-v'\frac{\partial \overline{T}}{\partial y} \approx -\mathbf{U}' \cdot \nabla \overline{T} \approx \left(\frac{\partial \overline{T}}{\partial z} + \frac{g}{C_p}\right)w'. \qquad (7)$$

In contrast, different balance holds near the surface. Strong meridional heat transport by the circulation anomalies cannot be compensated by weak adiabatic effects, which leaves significant imbalance between them (Fig. 8c). Over the Sea of Okhotsk, this near-surface thermal imbalance is compensated by diabatic processes associated with anomalous turbulent sensible and latent fluxes between the atmosphere and ocean. In fact, the anomalous sea-ice cover causes an enormous amount of the anomalous heat fluxes (Fig. 9).

c. Atmospheric responses in the thermal forcing region

In this section, we examine the dynamic and thermodynamic mechanisms that are involved in the wave formation of the mid- and upper troposphere due to the thermal forcing at the surface. We identify strong sensible and latent heat flux anomalies as primary heating (HS) and cooling (CS) sources for the large-scale wavelike response (Fig. 9). In the heavy ice case, sensible and latent heat release from the sea surface around the Kuril Islands and off the Kamchatka peninsula (HS) is greatly augmented, while it is suppressed over the Sea of Okhotsk (CS). The northerly wind anomalies over this HS near the Kamchatka peninsula are indicative of compensation of the heating by the near-surface cold advection (Fig. 8a). For an undamped steady response, the thermal balance near the surface where the mean wind is rather weak is approximated by

$$\mathbf{U}' \cdot \nabla \overline{T} \approx \frac{Q'}{C_p}, \qquad (8)$$

where Q' is the heating rate due to anomalous heat fluxes from the ocean. With this balance, a surface high should be located to the west of the HS (east of the CS) in quadrature with the anomalous heat fluxes. As the thermal forcing is confined to the lower layer, the high should be associated with cold air temperature. In reality, however, the shift of the surface high relative to the CS is substantially less than implied by (8), suggestive of significant contributions from thermal damping that act to generate positive (negative) temperature anomalies right over the shallow HS (CS). Thus, thermal damping acts to generate warm cyclonic (cold anticyclonic) anomalies right over HS (CS). In the actual AGCM response, the westward shift of the surface high relative to the HS generated in balance with the meridional temperature advection is substantially moderated by the thermal damping effect.

In view of the vorticity balance, the meridional wind anomalies near the surface give rise to planetary vorticity advection, which needs to be balanced in part by a low-level divergence/convergence effect, as indicated in (4). In addition, surface friction acts to weaken the shallow surface anomalous high. This effect is also compensated by the generation of negative vorticity associated with the low-level divergence. Thus, the anomalous low-level divergence spreads over the surface anticyclonic anomalies and extends farther to the east. The divergence requires the anomalous midlevel descent, which connects the lower- and upper-level circulation anomalies through the effect of anomalous upper-level convergence upon the vorticity balance. Positive vorticity generation due to this upper-level convergence needs to be compensated by the negative ζ' advection with the prevailing basic-state westerlies. This negative vorticity advection corresponds to anticyclonic and cyclonic anomalies to the west and east of the anomalous descent, respectively, in the mid- and upper troposphere, which indicates that phase of the upper-level wave train shifts to the west of the near-surface counterpart (e.g., Fig. 6). Thermodynamically, anomalous adiabatic warming associated with this anomalous descent tends to be balanced with the cold advection by the anomalous northerlies, which is again consistent with the westward shift of the anticyclonic anomalies relative to the anomalous descent.

d. Estimation of wave activity flux

To envisage the propagation of the stationary Rossby wave train of interest, we estimated the associated wave activity flux by applying Plumb's (1985) formula to the difference field (i.e., the heavy minus light composites). His flux, which is defined on the log pressure ($=z$) coordinate for the zonally averaged basic state, may be expressed as

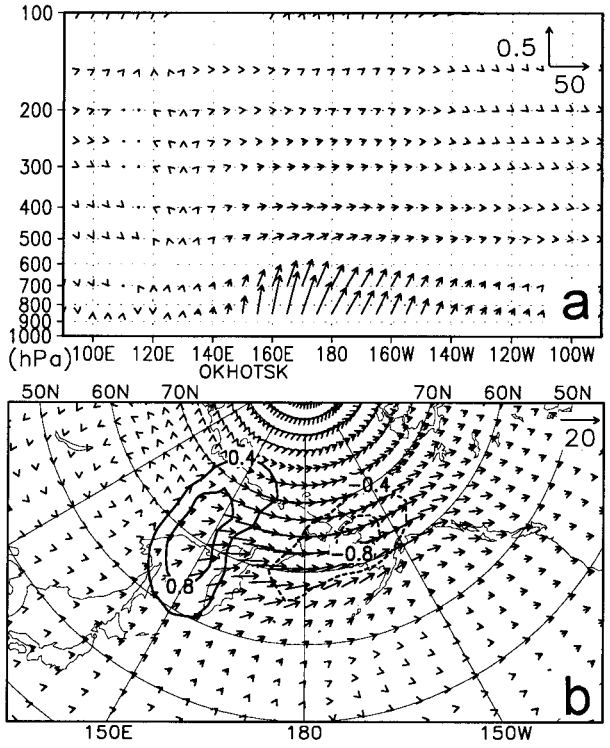

FIG. 10. Plumb's (1985) wave activity flux ($m^2\ s^{-2}$) estimated from the Jan–Feb mean difference fields of the AGCM simulations between the heavy and light ice cases. (a) Zonal cross section based on 50°–70°N average. (b) Distribution of the 500–200-hPa averaged horizontal flux ($m^2\ s^{-2}$; arrows), with its divergence/convergence superimposed (10^{-5} m s^{-2}; contours).

$$\mathbf{F}_S = p^* \cos\phi \times \left\{ \begin{array}{c} v'^2 - \dfrac{1}{2\Omega a \sin 2\phi}\dfrac{\partial(v'\Phi')}{\partial\lambda} \\ -u'v' + \dfrac{1}{2\Omega a \sin 2\phi}\dfrac{\partial(u'\Phi')}{\partial\lambda} \\ \dfrac{2\Omega \sin\phi}{S}\left[v'T' - \dfrac{1}{2\Omega a \sin 2\phi}\dfrac{\partial(T'\Phi')}{\partial\lambda}\right] \end{array} \right\}, \quad (9)$$

with

$$S = \frac{\partial T}{\partial z} + \frac{g}{C_p},$$

where u is the eastward wind component; Φ the geopotential height; Ω the earth's rotation rate; a the earth's radius; (ϕ, λ) latitude and longitude, respectively; and p^* pressure normalized by 1000 (hPa). Primes denote deviations from the zonal averages and a caret signifies averaging over the area to the north of 20°N. The flux, which is supposed to be parallel to the local group velocity in the almost plane wave limit, illustrates the three-dimensional propagation of a wave packet on the zonally uniform westerlies. As seen in Fig.10, $\mathbf{F}_s$ is indeed dominantly eastward, in the direction of the group velocity of stationary Rossby waves. The upward flux of wave activity is evident over the east of the Sea of Okhotsk with the strongly divergent horizontal component aloft, and no significant upward flux is observed upstream, which indicates that the wave train is forced and generated there.[1]

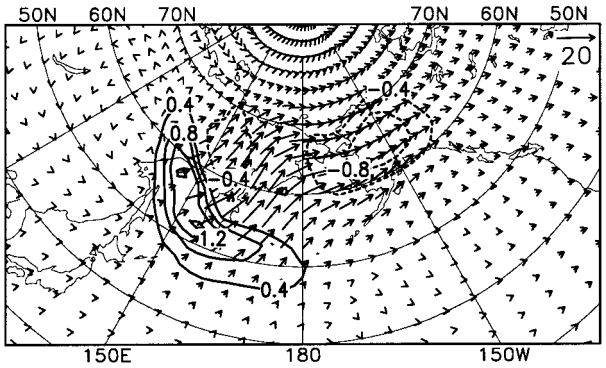

FIG. 11. As in Fig. 10b, but for Takaya and Nakamura's (1997) flux. The horizontal component is multiplied by pressure normalized by 1000 (hPa), so as to correspond to Plumb's (1985) formula.

The climatological mean flow meanders due to a deep trough above the Sea of Okhotsk and a ridge over the eastern Pacific (e.g., Fig. 3), which may significantly influence the wave propagation. This influence cannot be incorporated in Plumb's (1985) flux derived for the zonally uniform westerlies, but it can be in a flux generalized by Takaya and Nakamura (1997) for a zonally asymmetric basic state:

$$\mathbf{W} = \frac{1}{2|\overline{\mathbf{U}}|} \times \left\{ \begin{array}{c} U(\psi_x'^2 - \psi'\psi'_{xx}) + V(\psi'_x\psi'_y - \psi'\psi'_{xy}) \\ U(\psi'_x\psi'_y - \psi'\psi'_{xy}) + V(\psi'^2_y - \psi'\psi'_{yy}) \\ \dfrac{f^2}{S^2}[U(\psi'_x\psi'_p - \psi'\psi'_{xp}) + V(\psi'_y\psi'_p - \psi'\psi'_{yp})] \end{array} \right\}, \quad (10)$$

with

$$S^2 = -\alpha\frac{\partial(\ln\theta)}{\partial p},$$

where $\overline{\mathbf{U}}(U, V)$ denotes the mean wind vector, ψ' perturbation geostrophic streamfunction, θ potential temperature, p pressure, and α specific volume. As seen in Fig. 11, the overall pattern of $\mathbf{W}$ is similar to that of $\mathbf{F}_s$ in the sense that $\mathbf{W}$ and $\mathbf{F}_s$ both diverge out over the Sea of Okhotsk and are both dominantly eastward along the downstream wave train. A subtle but dynamically significant difference is that the horizontal divergence of $\mathbf{W}$ spreads mostly over the Sea of Okhotsk and off the Kamchatka peninsula, whereas the strong diver-

[1] A significant computational error was found in the estimation of the wave activity flux shown in Fig. 5 of Honda et al. (1996). The error has been corrected in Fig. 10 of the present paper.

gence of $\mathbf{F}_s$ extends from the Sea of Okhotsk into eastern Siberia. Obviously, the former corresponds to the primary heating and cooling sources better and looks more reasonable (Fig. 9). The above diagnosis by means of wave activity fluxes suggests that the stationary wavelike anomalies in the AGCM are Rossby waves forced by the anomalous heat flux from the ocean due to the anomalous sea-ice cover in the Sea of Okhotsk.

3. Observational results

Observational data used in this study consist of the following fields for the Northern Hemisphere, based on the National Meteorological Center (NMC; now the National Centers for Environmental Prediction) operational analyses archived in the National Center for Atmospheric Research data library: SLP, surface air temperature (T_s), 500-hPa height (Z_{500}), and 500-hPa p-velocity (ω_{500}). They are archived on the 1977-point octagonal grid that covers the entire area north of 20°N. Twice-daily data are available throughout the period January 1973–March 1994, except for ω_{500}, which is available since September 1975. We also used the Japan Meteorological Agency Okhotsk sea-ice grid data, based on Environmental Science Services Administration, National Oceanic and Atmospheric Administration, and Geostationary Meteorological Satellite satellite images (e.g., Kano et al. 1989). Horizontal resolution is 0.25° both in latitude and longitude, and 5-day mean data for winter (December–May) are available for the period 1970–94. We focus on the situation in February, the time of the year when the ice cover in the Sea of Okhotsk becomes most extensive and presumably its impact on the atmosphere, if it exists, is likely to be strongest.

The wintertime atmospheric circulation over the North Pacific and the marginal sea tends to be influenced strongly by El Niño–Southern Oscillation (ENSO) events. Therefore, when we analyze the observational data, phenomena of interest may be hidden behind the remote response to ENSO. In this study, we attempt to remove most of the ENSO influence from the atmospheric fields over the North Pacific, following Zhang et al. (1996). First, we computed the linear regression coefficient between the Southern Oscillation index (SOI), defined as the SLP difference between Tahiti and Darwin, and a particular meteorological variable at each grid point for the 22-yr period. For each year the January–March mean value was analyzed in order to remove intraseasonal fluctuations. We then defined a ''hypothetical'' ENSO response at each grid point in the extratropics as a product of the local regression coefficient and the 3-month mean SOI value for a particular year. The ''residual'' field, computed by subtracting the hypothetical ENSO response from the observed anomaly field for February of the year, should be linearly independent of the ENSO signal and dominated by midlatitude processes. The underlying hypothesis of this method is that the extratropical response to ENSO is approximately a linear function of the ENSO signal. Of course, the residual field is by no means completely free from the influence of the tropical interannual variability due to nonlinearity of the extratropical response to ENSO and to tropical forcing other than ENSO. Still, in the residual field, the noise has been substantially reduced in detecting the signal generated by the sea-ice cover anomalies over the Sea of Okhotsk.[2]

We have shown through the numerical experiments in section 2 that significant stationary response to the anomalous sea-ice cover in the Sea of Okhotsk is brought about by a pair of heating and cooling sources associated with anomalous sensible and latent heat fluxes to the atmosphere. The cooling source tends to be strong when the Sea of Okhotsk is mostly covered with sea ice that greatly suppresses the sensible and latent heat release from the surface. The heating source tends to be intensified by the enhanced heat fluxes from the ocean surface due to the strong northerly offshore winds off the abnormally extended ice cover. Although the ice cover in the model is fixed throughout the winter, such strong offshore winds, in reality, should act to further extend the ice cover and would therefore be reflected by the increasing ice cover in the observed data. We hence hypothesize that the atmospheric signal associated with the heavy ice cover is observed most clearly when the sea-ice area is most extensive and exhibits a strong increasing tendency as well. Likewise, the atmospheric signal associated with the light ice cover is supposed to be most apparent when the ice cover is least extensive and/or it exhibits an obvious decreasing tendency. Figure 12 shows a relationship between the largest sea-ice area in February within the Sea of Okhotsk and the tendency of the sea-ice area during February for years 1973–94. Based on the hypothesis mentioned above, the 22 yr are classified into three categories: 1) heavy ice years, 2) light ice years, and 3) other years. Although six years are labeled to be light ice years, we select four years out of them that correspond to the four least extents of the ice area. There is no significant difference between the 4- and 6-yr mean fields. Atmospheric fields (or anomalies) were composited for the four winters for the heavy and light ice cover cases, separately, in order to extract the coherent signal associated with the sea-ice anomalies.

In the composite maps (not shown), characteristics of both cases are in good agreement with those in the AGCM simulation (Figs. 2 and 3), though the observed differences are somewhat less apparent than in the sim-

[2] Extratropical wind and temperature anomalies associated with ENSO could change the sea-ice extent in the Sea of Okhotsk. The response of the midlatitude atmosphere to this sea-ice change, if it exists, then could in turn modify the atmospheric anomalies that have been forced directly from the Tropics. In the present study, we do not attempt to isolate this indirect influence of ENSO via sea-ice anomalies.

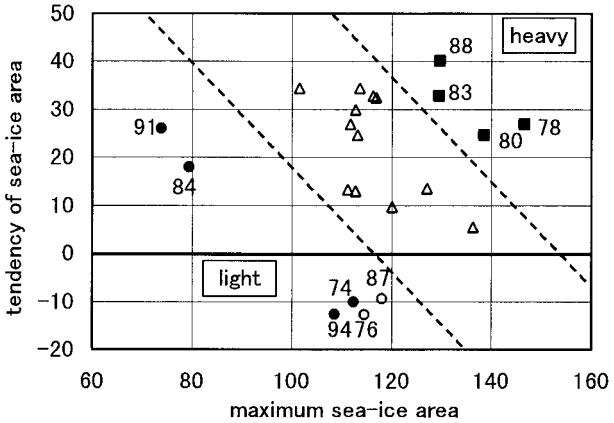

FIG. 12. Scatter diagram showing the relationship between the maximum Okhotsk sea-ice area during Feb based on 5-day mean fields and the tendency of that ice area during Feb (subtracted last 5-day mean in Jan from that in Feb) for individual years from 1973 to 1994, as indicated by their last two digits (e.g., 80 denotes the year 1980). Closed square: heavy ice years; closed circle: light years (included in the composites); open circle: light years (not included); and open triangle: other years. Units: 10^4 km^2 for both axes.

ulation. We then attempt to extract the atmospheric anomalies associated with the Okhotsk sea-ice anomalies by subtracting the 4-yr composite of a particular variable for the light ice case from the counterpart for the heavy ice case. The composite difference map for SLP (Fig. 13a) is characterized by anticyclonic anomalies over the Sea of Okhotsk and Japan and stronger cyclonic anomalies over the northern North Pacific and the Bering Sea. In the difference map for T_s (Fig. 13b), the Sea of Okhotsk is covered with cold anomalies and the more intense warm anomalies over Alaska and the Bering Strait. At the 500-hPa level (Fig. 14a), prominent wavelike anomalies are evident in the difference field of Z_{500} with anticyclonic anomalies to the south of Japan and Alaska, and negative ones over the Kamchatka peninsula and the Aleutian Islands. Anomalous descent over the Sea of Okhotsk and the western United States and anomalous ascent over the Bering Sea and Strait dominate the difference field of ω_{500} (Fig. 14b). The pattern of the ω_{500} anomalies implies anomalous low-level divergence just above the cold anticyclonic anomalies over the Sea of Okhotsk and anomalous low-level convergence just above the warm cyclonic anomalies to the east of the Kamchatka peninsula. These statistically significant characteristics in the difference fields correspond well to the counterpart in the AGCM experiments (Figs. 2–5), though again the observed differences are less intense and also less significant statistically than those simulated.

In the real atmosphere, a signal forced by sea-ice anomalies may be masked not only by the dominant remote influence of ENSO and such internally generated interannual variability as the Arctic Oscillation (Kodera et al. 1996; Thompson and Wallace 1998), but also by the atmospheric anomalies that have given rise to the

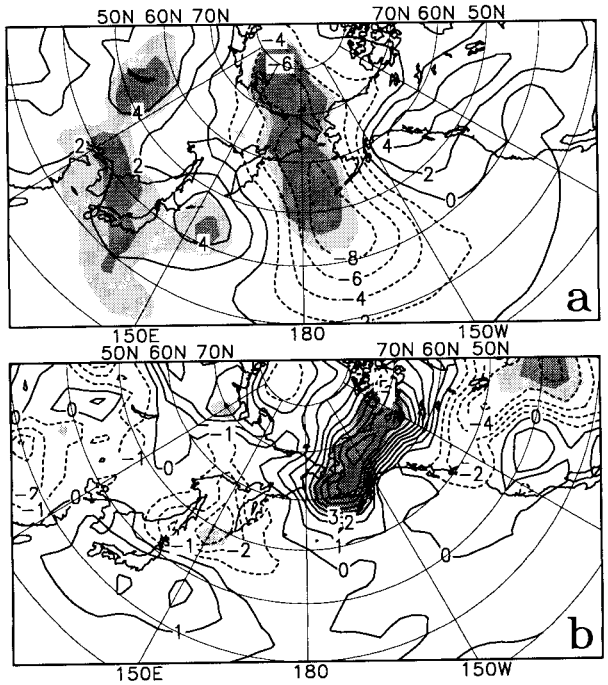

FIG 13. Composite differences of (a) sea level pressure (hPa) and (b) surface air temperature (°C) between the four heaviest ice years (1978, 1980, 1983, and 1988) and four lightest ice years (1974, 1984, 1991, and 1994), based on the NMC operational analyses for Feb (the heaviest minus the lightest). Light and heavy shadings indicate the differences with 90% and 95% confidence levels, respectively.

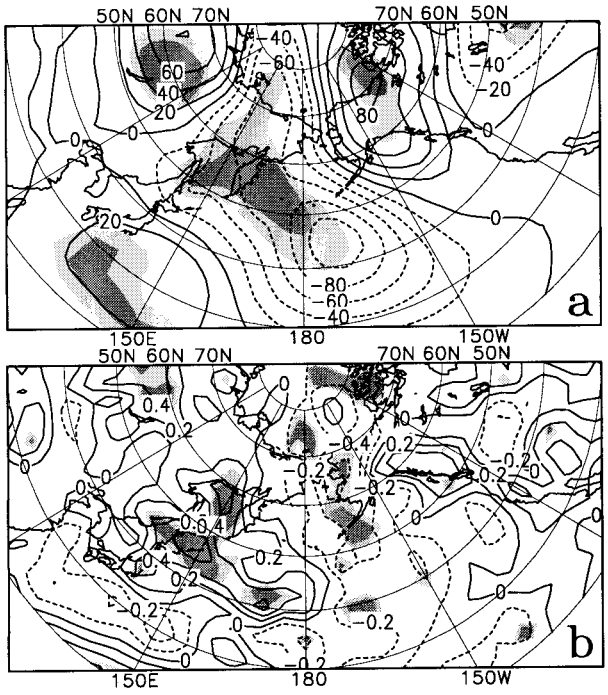

FIG. 14. As in Fig. 13, but for 500-hPa (a) geopotential height (m) and (b) p velocity (10^{-1} Pa s^{-1}).

sea-ice anomalies themselves (Fang and Wallace 1994; Honda et al. 1994). For this reason, we needed to impose fairly strict criteria in differentiating observed sea-ice conditions, so as to extract the atmospheric signal to the Okhotsk sea-ice anomalies in the clearest manner as possible. In fact, using the February mean sea-ice area in place of the maximum sea-ice area in that month lowered the statistical significance in the composite difference, although the anomaly pattern itself is similar. Furthermore, differentiating the observed heavy and light ice conditions based only on the maximum sea-ice area in February without the increasing tendency of the ice area failed to capture any significant signal. Of course, our result based on a rather small sample size (22 yr) is probably not sufficiently robust. Nevertheless, the atmospheric anomalies extracted in the composite difference maps on the basis of our criteria are in the form of a wave train emanating from the vicinity of the Sea of Okhotsk, as simulated in the AGCM. Our analysis of the observed data seems to capture the atmospheric response to the Okhotsk ice anomalies, although the differences between the observed and simulated anomalies around the Sea of Okhotsk may manifest the atmospheric anomalies that gave rise to the largest ice cover and the strongest expanding tendency.

4. Conclusions

We performed a numerical experiment using an AGCM, to examine the influence of Okhotsk sea-ice extent anomalies on the large-scale atmospheric circulation and to understand the dynamic and thermodynamic characteristics of the atmospheric response. Significant differences between the heavy and light ice cases are evident in the response not only around the Sea of Okhotsk, but also far downstream in the form of a stationary wave train propagating along a great circle. The anomalous sea-ice cover causes the near-surface anomalous diabatic heating, which yields a stationary low-level response that compensates the heating with both thermal damping and temperature advection by the induced meridional wind anomalies. The latter also advects the planetary vorticity. The vorticity balance requires anomalous low-level divergence and thus a descent aloft over and to the east of the near-surface cold anticyclonic anomalies. The anomalous vertical motion thus induced acts as a ''communicator'' between the low-level thermal response and upper-level wavelike response. The phase relation between them is determined in such a way that the upper-level advection of anomalous relative vorticity by the prevailing mean westerlies is balanced with the divergence effect associated with the anomalous vertical motion. Hence, cyclonic anomalies aloft appear to the east of the anomalous descent and near-surface divergence. This particular phase alignment in the upper-level wave train also satisfies the midtropospheric thermodynamic balance, as the adiabatic heating associated with the vertical motion is compensated by the temperature advection by the meridional wind anomalies. A diagnosis by means of wave activity fluxes strongly suggests that the response is a stationary Rossby wave train forced thermally by the anomalous surface heat fluxes around the Sea of Okhotsk.

In the AGCM response, significant upward wave activity flux is discernible in the lower troposphere not only above the primary heating and cooling sources over the Sea of Okhotsk and off the Kamchatka peninsula, but also farther downstream over the Bering Sea and the Gulf of Alaska (Fig. 10a). This reflects near-surface temperature anomalies and associated low-level poleward heat fluxes along the wave train (Fig. 4). Since the remote stationary response is, by nature, equivalent barotropic, even in the vertically sheared westerlies (Held et al. 1985), the near-surface temperature anomalies downstream of the primary heating and cooling sources must be generated by thermal damping through anomalous atmosphere–ocean heat exchange. Specifically, the anomalous southerlies around the Alaskan Pacific coast associated with the remote barotropic response give rise to anomalous warm air advection across a strong low-level thermal contrast along the coast. In the steady response, this warm advection is in balance with less upward heat flux from the ocean surface where the temperature is prescribed (Fig. 9), in association with warm air temperature anomalies trapped near the surface (Fig. 4b). Energetically, the poleward heat fluxes across the equatorward temperature gradient mean the generation of eddy available potential energy, which is considered to be converted into eddy kinetic energy through the lower-tropospheric vertical heat flux. In fact, near-surface temperature anomalies (Fig. 4) are correlated positively with low-level vertical motion (Fig. 6, also Fig. 5b) along the wave train in the AGCM response. Furthermore, in the observed atmospheric anomalies related to the Okhotsk sea-ice anomalies, near-surface temperature anomalies in Fig. 13b are also correlated positively both with anomalous meridional and with vertical velocities at the lower levels, as inferred from Figs. 13 and 14. These low-level poleward and vertical heat fluxes associated with the remote response may hint that reinforcement of Rossby waves due to a destabilizing effect of thermal damping, as discussed in Held et al. (1986), is operative both in the AGCM and in the real atmosphere.

It should be borne in mind that the atmospheric response to the Okhotsk sea-ice anomalies simulated in our AGCM is presumably exaggerated to a certain extent. In reality, unlike as specified in the AGCM, a sea-ice area includes leads and polynyas. Although they occupy a small fraction of the total ice cover, they contribute to the effective transport of heat and moisture from the underlying sea to the atmosphere and thereby act to reduce the contrast in the transport between the open ocean and ice-covered area. Furthermore, SSTs over the open ocean are fixed to the climatological means in the AGCM, despite the tendency of the SSTs,

in reality, to change so as to minimize the heat exchange to the atmosphere above (Alexander 1992). For example, the cold offshore winds in front of the ice edge lower SSTs, which leads to the weakening of the primary heating source for the atmospheric response. Likewise, the reinforcement of the remote response due to the thermal damping by the prescribed SSTs, if it exists, should be overestimated because of the same adjustment as above acting on SSTs of the real ocean. For these reasons, the surface heat fluxes are likely to be somewhat overestimated in the model compared to the observation (e.g., Esbensen and Kushnir 1981; Oberhuber 1988). The adjustment as above could change the SST only by several degrees in magnitude. The change, however, is much less than a typical surface temperature contrast between the open ocean and the sea ice. Therefore it is unlikely that the adjustment substantially suppresses the atmospheric response to the sea-ice anomalies.

Anomalous heat and moisture supply from the surface due to anomalous sea-ice cover could alter the distribution of clouds whose radiative effects may modify the distribution of anomalous diabatic heating (e.g., Curry et al. 1996; Randall et al. 1998). In our difference composites for the heavy ice cover relative to the light ice cover, cloud cover tends to decrease slightly over the anomalously extended sea ice over the Sea of Okhotsk and to the east of the ice edge. It tends to increase slightly over the Bering Sea due to the increased moisture advection by the anomalous southerlies. The corresponding anomalous radiative heating and cooling appear in the former and latter maritime regions, respectively. Neither of them, however, exceeds 30 W m^{-2}, which is nearly an order less than the anomalous heat supply through the turbulent fluxes and therefore negligible in our simulation. It should be noted that parameterizations for the formation of clouds and their radiative properties must be insufficient in our model, particularly in the lower troposphere. Hence, an AGCM with a higher spatial resolution and improved parameterizations should be used in the future for a more quantitative argument on the cloud feedback on the atmospheric response to anomalous sea-ice cover.

In view of the sensitivity of the midlatitude atmospheric circulation to the lower boundary conditions, the present result is consistent with those of AGCM sensitivity experiments to the midlatitude SST anomalies in the northwestern Atlantic (e.g., Palmer and Sun 1985) and in the northwestern Pacific (e.g., Peng et al. 1997; Peng and Whitaker 1999). In these two regions, meridional T_s gradients are strong, and heat fluxes from the ocean surface to the atmosphere are pronounced. In the mean state, meridional T_s gradients are also strong in the vicinity of the Sea of Okhotsk. The prevailing offshore northerlies cause pronounced sensible and latent heat fluxes from the ocean surface off the sea-ice edge. The heat flux distribution must vary sensitively in association with interannual and even intraseasonal anomalies in the Okhotsk sea-ice extent. The present study suggests that the heat flux anomalies in and around the Sea of Okhotsk are capable of causing a remote response by emanating a stationary Rossby wave train downstream. As the location of the Pacific storm track simulated in the AGCM is too far south of the Sea of Okhotsk, there is little contribution of the feedback of the transients to the model remote response.

It has been shown that sea-ice cover anomalies in the eastern Sea of Okhotsk tend to be out of phase with those in the eastern Bering Sea (Cavalieri and Parkinson 1987; Fang and Wallace 1994). The seesaw in the sea-ice cover may be related to the tendency of the direction of interannual wind anomalies over the Sea of Okhotsk to be opposite to that over the Bering Sea, in association with the interannual variability in the position and intensity of the Aleutian low. In our model simulation (Fig. 2), the surface southeasterlies prevailing over the eastern Bering Sea in the heavy Okhotsk ice case act to suppress the ice extension locally, whereas the surface northeasterlies in the light Okhotsk ice case act to enhance the ice extension. The simulated surface temperature anomalies also contribute positively to these tendencies in the eastern Bering ice cover (Fig. 4b). Results of our AGCM experiments suggest that the observed pattern of the wind anomalies may be associated with a wavelike atmospheric response forced by the anomalous sea-ice cover over the Sea of Okhotsk. Hence, the seesaw-like variability in sea-ice cover between the two seas may be, at least in part, a manifestation of the ''atmospheric bridge'' as an atmospheric remote response to the Okhotsk sea-ice anomalies.

Acknowledgments. We would like to thank Drs. Yoshihiro Tachibana and Jinro Ukita for heated discussion and encouragement throughout this study. We also thank Dr. Masaru Chiba for his technical support in numerical experiments using AGCM. Our numerical model integrations were carried out on a HITAC S-3800/300 at the Hokkaido University Computing Center and on a Cray T932 at National Research Institute for Earth Science and Disaster Prevention. The Grid Analysis and Display System (GrADS) was used for drawing the figures. One of the authors (M.H.) was supported by Research Fellowships of the Japan Society for the Promotion of Science for Young Scientists. A major portion of this work is based on a Ph.D. dissertation of M.H. at Hokkaido University. This work was supported in part by a Grant-in-Aid for Scientific Research from the Japanese Ministry of Education, Science and Culture, and by a Grant-in-Aid for Cooperative Research from Center for Climate System Research, University of Tokyo.

REFERENCES

Agnew, T., 1993: Simultaneous winter sea-ice and atmospheric circulation anomaly patterns. *Atmos.–Ocean,* **31,** 259–280.

Alexander, M. A., 1992: Midlatitude atmosphere–ocean interaction during El Niño. Part I: The North Pacific Ocean. *J. Climate,* **5,** 944–958.

Aso, T., 1986: Ohôtsuku-kai no kaihyô bumpu to kishô (Distribution of sea ice and weather conditions in the Sea of Okhotsk). *Gijutsu Jiho Bessatsu,* **35,** 5–14.

Cavalieri, D. J., and C. L. Parkinson, 1987: On the relationship between atmospheric circulation and fluctuations in the sea ice extents of the Bering and Okhotsk seas. *J. Geophys. Res.,* **92,** 7141–7162.

Chiba, M., K. Yamazaki, K. Shibata, and Y. Kuroda, 1996: The description of the MRI Atmospheric Spectral GCM (MRI-GSPM) and its mean statistics based on 10-year integration. *Pap. Meteor. Geophys.,* **47,** 1–45.

Crane, R. G., 1978: Seasonal variations of sea ice extent in the Davis Strait–Labrador Sea area and relationships with synoptic-scale atmospheric circulation. *Arctic,* **31,** 434–447.

Curry, J. A., W. B. Rossow, D. A. Randall, and J. L. Schramm, 1996: Overview of Arctic cloud and radiation characteristics. *J. Climate,* **9,** 1731–1764.

Esbensen, S. K., and Y. Kushnir, 1981: *The Heat Budget of the Global Ocean: An Atlas Based on Estimates from Surface Marine Observations.* Climate Research Unit, Oregon State University, Corvallis, OR, 27 pp. and figs.

Fang, Z., and J. M. Wallace, 1994: Arctic sea ice variability on a timescale of weeks and its relation to atmospheric forcing. *J. Climate,* **7,** 1897–1914.

Held, I. M., R. L. Panetta, and R. T. Pierrehumbert, 1985: Stationary external Rossby waves in vertical shear. *J. Atmos. Sci.,* **42,** 865–883.

——, R. T. Pierrehumbert, and R. L. Panetta, 1986: Dissipative destabilization of external Rossby waves. *J. Atmos. Sci.,* **43,** 388–396.

Herman, G. F., and W. T. Johnson, 1978: The sensitivity of the general circulation to Arctic sea ice boundaries: A numerical experiment. *Mon. Wea. Rev.,* **106,** 1649–1664.

Honda, M., Y. Tachibana, and M. Wakatsuchi, 1994: The influences of the sea ice and the wind field on the winter air temperature variation in Hokkaido. *Proc. NIPR Symp. Polar Meteor. Glaciol.,* **8,** 81–94.

——, K. Yamazaki, Y. Tachibana, and K. Takeuchi, 1996: Influence of Okhotsk sea-ice extent on atmospheric circulation. *Geophys. Res. Lett.,* **23,** 3595–3598.

Kano, Y., K. Sato, and S. Shirato, 1989: Statistical study on sea ice in the Okhotsk Sea observed by GMS for 10 years. *Oceanogr. Mag.,* **39,** 43–58.

Kodera, K., M. Chiba, H. Koide, A. Kitoh, and Y. Nikaidou, 1996: Interannual variability of the winter stratosphere and troposphere in the Northern Hemisphere. *J. Meteor. Soc. Japan,* **74,** 365–382.

Louis, J. F., 1979: A parametric model of vertical eddy fluxes in the atmosphere. *Bound.-Layer Meteor.,* **17,** 187–202.

Nagata, M., and M. Ikawa, 1988: Numerical experiments of the convergent cloud band over the Japan Sea (in Japanese). *Tenki,* **35,** 151–155.

Niebauer, J., 1980: Sea ice and temperature variability in the eastern Bering Sea and the relation to the atmospheric fluctuations. *J. Geophys. Res.,* **85,** 7507–7516.

Oberhuber, J. M., 1988: The budget of heat, buoyancy and turbulent kinetic energy at the surface of the global ocean. Max-Planck Institut für Meteorologie Rep. 15, 19 pp. and figs. [Available from Max-Planck Institut für Meteorologie, Bundesstrasse 55, 20147 Hamburg, Germany.]

Okubo, H., and N. Mannoji, 1994: The influence of the sea ice distribution on the surface wind forecast by Japan Spectral Model (in Japanese). *Tenki,* **41,** 847–851.

Overland, J. E., and C. H. Pease, 1982: Cyclonic climatology of the Bering and its relation to sea ice extent. *Mon. Wea. Rev.,* **110,** 5–13.

Palmer, T. N., and Z. Sun, 1985: A modelling and observational study of the relationship between sea surface temperature in the northwest Atlantic and the atmospheric general circulation. *Quart. J. Roy. Meteor. Soc.,* **111,** 947–975.

Parkinson, C. L., 1990: The impact of the Siberian high and Aleutian low on the sea-ice cover of the Sea of Okhotsk. *Ann. Glaciol.,* **14,** 226–229.

Peng, S., and J. S. Whitaker, 1999: Mechanisms determining the atmospheric response to midlatitude SST anomalies. *J. Climate,* **12,** 1393–1408.

——, W. A. Robinson, and M. P. Hoering, 1997: The modeled atmospheric response to midlatitude SST anomalies and its dependence on background circulation states. *J. Climate,* **10,** 971–987.

Plumb, R. A., 1985: On the three-dimensional propagation of stationary waves. *J. Atmos. Sci.,* **42,** 217–229.

Randall, D., and Coauthors, 1998: Status of and outlook for large-scale modeling of atmosphere–ice–ocean interactions in the Arctic. *Bull. Amer. Meteor. Soc.,* **79,** 197–219.

Rogers, J. C., 1978: Meteorological factors affecting interannual variability of summertime ice extent in the Beaufort Sea. *Mon. Wea. Rev.,* **106,** 890–897.

Sasaki, H., and S. Deguti, 1988: Numerical experiments of the convergent band formed off the western coast of Hokkaido in winter (in Japanese). *Tenki,* **35,** 723–729.

Takaya, K., and H. Nakamura, 1997: A formulation of a wave-activity flux for stationary Rossby waves on a zonally varying basic flow. *Geophys. Res. Lett,* **24,** 2985–2988.

Thompson, D. W. J., and J. M. Wallace, 1998: The Arctic Oscillation signature in the wintertime geopotential height and temperature fields. *Geophys. Res. Lett,* **25,** 1297–1300.

Walsh, J. E., and C. M. Johnson, 1979: Interannual atmospheric variability and associated fluctuations in Arctic sea ice extent. *J. Geophys. Res.,* **84,** 6915–6928.

——, and J. E. Sater, 1981: Monthly and seasonal variability in the ocean-ice-atmosphere systems of the North Pacific and North Atlantic. *J. Geophys. Res.,* **86,** 7425–7445.

Zhang, Y., J. M. Wallace, and N. Iwasaka, 1996: Is climate variability over the North Pacific a linear response to ENSO? *J. Climate,* **9,** 1468–1478.